NeuroImage: Clinical 30 (2021) 102580

Contents lists available at ScienceDirect

NeuroImage: Clinical

journal homepage: www.elsevier.com/locate/ynicl

Focal cervical spinal stenosis causes mechanical strain on the entire cervical spinal cord tissue – A prospective controlled, matched-pair analysis based on phase-contrast MRI

Katharina Wolf [a,*], Marco Reisert [b], Saúl Felipe Beltrán [a], Jan-Helge Klingler [c], Ulrich Hubbe [c], Axel J. Krafft [b], Karl Egger [d,e], Marc Hohenhaus [c]

[a] Department of Neurology and Neurophysiology, Medical Center – University of Freiburg, Faculty of Medicine, University of Freiburg, Germany
[b] Department of Radiology, Medical Physics, Medical Center – University of Freiburg, Faculty of Medicine, University of Freiburg, Germany
[c] Department of Neurosurgery, Medical Center – University of Freiburg, Faculty of Medicine, University of Freiburg, Germany
[d] Department of Neuroradiology, Medical Center – University of Freiburg, Faculty of Medicine, University of Freiburg, Germany
[e] Department of Radiology, Tauernklinikum Zell am See/Mittersill, Salzburg, Austria

ARTICLE INFO

Keywords:
Phase-contrast MRI
Automated segmentation
Spinal cord
Degenerative cervical myelopathy
Convolutional neural network

ABSTRACT

Background: Focally increased spinal cord motion at the level of cervical spinal stenosis has been revealed by phase-contrast MRI (PC-MRI).
Objective: To investigate spinal cord motion among patients suffering of degenerative cervical myelopathy (DCM) across the entire cervical spine applying automated segmentation and standardized PC-MRI post-processing protocols.
Methods: Prospective, matched-pair controlled trial on 29 patients with stenosis at C5/C6. MRI-protocol covering all cervical segments: 3D T2-SPACE, prospectively ECG-triggered sagittal PC-MRI. Segmentation by trained 3D hierarchical deep convolutional neural network and data processing were conducted via in-house software pipeline. Parameters per segment: maximum velocity, peak-to-peak (PTP)-amplitude, total displacement, PTP-amplitude^{HB} (PTP-amplitude per duration of heartbeat), and, for characterization of intraindividual alterations, the PTP-amplitude index between the cervical segments C3/C4–C7/T1 and C2/C3.
Results: Spinal cord motion was increased at C4/C5, C5/C6 and C6/C7 among patients (all parameters, $p < 0.001$–0.025). The PTP-amplitude index revealed an increase from C3/C4 to C4/C5 ($p = 0.002$), C4/C5 to C5/C6 ($p = 0.037$) and a decrease from C5/C6 to C6/C7 and C6/C7 to C7/T1 ($p < 0.001$, each). This implied an up-building stretch on spinal cord tissue cranial and a mechanical compression caudal of the stenotic level. Furthermore, significant far range effects across the entire cervical spinal cord were observed (e.g. PTP-amplitude C2/C3 vs. C6/C7, $p = 0.026$) in contrast to controls ($p = 1.00$).
Conclusion: This study revealed the nature and extends of mechanical stress on the entire cervical spinal cord tissue due to focal stenosis. These pathophysiological alterations of spinal cord motion can be expected to be clinically relevant.

1. Introduction

Within the field of degenerative cervical myelopathy (DCM) altered dynamic effects within the spinal canal revealed by phase-contrast MRI (PC-MRI) are currently gaining interest as a possible new diagnostic parameter (e.g. Bunck et al., 2011; Wolf et al., 2018). PC-MRI allows a non-invasive quantitative evaluation of motion without application of contrast agents (Markl et al., 2012; Dyverfeldt et al., 2015; Yamada

Abbreviations: aMCC, adapted maximum canal compromise; AUC, area under the curve; C, cervical; CNN, convolutional neural network; CSA, cross-sectional area; CSF, cerebrospinal fluid; DCM, degenerative cervical myelopathy; DI, displacement index; HB, heartbeat; ICC, intra-class correlation coefficient; MRI, magnetic resonance imaging; n/nd, non-/normally distributed; pAI, Peak-to-peak-amplitude index; PC-MRI, phase-contrast MRI; PTP, peak-to-peak; ROI, region of interest; SD, standard deviation; T, thoracic; VENC, velocity encoding parameter.

* Corresponding author at: Department of Neurology and Neurophysiology, Breisacher Str. 64, D-79106 Freiburg, Germany.
E-mail address: katharina.wolf@uniklinik-freiburg.de (K. Wolf).

https://doi.org/10.1016/j.nicl.2021.102580
Received 26 October 2020; Received in revised form 30 November 2020; Accepted 21 January 2021
Available online 1 February 2021

et al., 2015). Among affected patients, the motion of the spinal cord assessed by PC-MRI was significantly increased at level of cervical stenosis (Wolf et al., 2018; Vavasour et al., 2014; Chank et al., 2014). Studying spinal cord motion targets directly the neural tissue at risk. Within a small number of DCM-patients, increased spinal cord motion has been related to impaired sensory evoked potentials (Vavasour et al., 2014) and functional impairment (Wolf et al., 2018). Thus, dynamic stress due to spinal cord motion seems to contribute to spinal cord deterioration. This new dynamic approach might improve diagnostic pathways, especially at early stages of DCM, depicting patients at risk to progress. Up to date, it remains unclear how spinal cord dynamics evolve across the entire cervical spinal cord within DCM-patients. Also, due to its novelty, fully standardized, automated and evaluated PC-MRI analysis procedures are sparse within the field of clinical research on spinal cord motion (e.g. manual segmentation (Wolf et al., 2018; Vavasour et al., 2014; Hupp et al., 2019), no analysis of measurement reliability (Vavasour et al., 2014; Chank et al., 2014), no phase-drift-correction (Wolf et al., 2018; Vavasour et al., 2014; Chank et al., 2014, etc.).

We hypothesized, that a relevant alteration of spinal cord dynamics across the whole cervical spine could be revealed by PC-MRI. Also, we aimed to introduce automated MRI-segmentation and data-processing for a more standardized approach.

2. Methods

2.1. Study design

This is a monocentric prospective controlled study. 29 DCM-patients with monosegmental relevant spinal stenosis at C5/C6 were withdrawn from a large cohort of an ongoing longitudinal trial (German registry of clinical trials, number: DRKS00012962). Relevant stenosis was defined as diminished CSF-space in the anterior or posterior compartments diagnosed in T2-weighted MRI. Protrusions at other levels were accepted (Figure Supplementary figure 1). An age- and gender-paired-matched cohort of 29 healthy controls was extracted of our database and adjoined for group comparison (German registry of clinical trials, number: DRKS00017351). Patients were recruited within our in-house ambulatories, controls by in-house advertisement. In- and exclusion criteria were reported before (Wolf et al., 2019). Controls presenting with unaware neurological symptoms, or patients presenting with conflicting neurological symptoms were prospectively excluded by an interview and a neurological exam before admission to the study. Severity of affection was scored via the modified Japanese Orthopedic Association score (mJOA) (Kato et al., 2015). The local ethic committee approved the trials on patients and healthy volunteers (Vote numbers: 261/17, 338/17); written informed consent of each participant was received. The data was collected between June 2018 and December 2019.

2.2. Imaging protocol

Each participant received one MRI scan (3T, SIEMENS MAGNETOM Prisma, SIEMENS Erlangen). The details of the applied MRI-sequences have been reported before (Wolf et al., 2019). In short, besides a standard 3D T2 SPACE sequence for anatomical imaging (spatial resolution $0.64 \times 0.64 \times 1.0$ mm^3), a prospectively ECG-triggered PC-MRI sequence in sagittal orientation was applied covering vertebra C1 to T1 with a spatial resolution of 0.62×0.62 mm^2 and a slice thickness of 3 mm. The velocity encoding parameter (VENC) was 5 cm/s. An approximated number of 40 time-points per heartbeat was collected. During the execution of the PC-MRI sequence, the average duration of the heartbeat (ms) per individual was automatically recorded. Average scanning time of the PC-MRI sequence was about 2 min depending on the heart rate.

2.3. MRI data processing

Segmentation of the subarachnoid space and the spinal cord were based on the T2-weighted sequence. As initial step in order to train a 3D hierarchical deep convolutional neural network (CNN), segmentations were manually generated on five patients, each by two experienced clinicians (KW, MH) using the medical imaging platform NORA (www.nora-imaging.org, nora-imaging). Applying in-house machine learning algorithms, these segmentations were used to train a CNN on the 3D T2-weighted sequences, whose implementation is similar as reported by Zhao et al. (2019) (Fig. 1). Since misregistrations between the 3D T2-weighted and the 2D PC-MRI sequences were observed (due to slight movement of the participant within the scanner), an additional CNN needed to be trained on the 2D PC-MRI sequences in order to gain reliable dynamic data of the spinal cord. 20 well aligned images were used to generate the new 2D groundtruth.

The cervical segments were defined by labeling the spinal cord at the level of the vertebra bodies (C2–C7) on the T2-weighted images (Fig. 1). With this information, a standardized region of interest (ROI) was automatically generated covering the central 1/3 of the spinal cord volume between two cervical vertebra bodies. Thus, each ROI covered the spinal cord tissue in front of each intervertebral disc as typical location of maximum spinal canal narrowing (Fig. 1). In total, six ROIs were analyzed per individual: one between vertebras C2/C3, C3/C4, C4/C5, C5/C6, C6/C7, and C7/T1, respectively. An additional ROI within non-moving dorsal neck muscle tissue was automatically generated per segment for phase drift correction (Gatehouse et al., 2012).

2.4. PC-MRI parameters

The following parameters of the spinal cord velocity curve per heartbeat were analyzed per ROI based on the PC-MRI sequence (Fig. 2): maximum velocity (cm/s) and peak-to-peak (PTP)-amplitude (mm/s). Additionally, the software computed the total displacement over one heartbeat (mm) by integration (~area under the curve (AUC), but addition of inversed negative AUC-values instead of subtraction). The total displacement combines information on the individual spinal cord velocity *and* the individual's duration of the heartbeat, which has been described to influence the intraspinal dynamics (Enzmann and Pelc, 1992; Bradley et al., 2016) (Fig. 2).

As an alternative parameter, that includes information of the velocity curve and the duration of the heartbeat, the PTP-amplitude^{HB} (mm) [PTP-amplitude (mm/s) × heartbeat (s)], was introduced.

Also, the PTP-amplitude index (pAI) was calculated per segment in relation to the segment C2/C3 as furthermost point from the stenosis ([PTP-amplitude$_{C3/4\ -\ C7/T1)}$ ÷ PTP-amplitude$_{C2/3}$]). As already discussed before, an index should be less sensitive to unknown or suspected interindividual differences (e.g. body size, spinal canal size) (Wolf et al., 2018). Also, the pAI allows conclusions on the mechanical strain on the spinal cord tissue: in case of a high index, the caudal spinal cord segment would move faster than the spinal cord at segment C2/C3, resulting in a stretch of the spinal cord tissue. A lower index would indicate a comparably slower motion and therefore a compression of the interjacent spinal cord (Fig. 3).

2.5. Anatomic MRI parameters

The following anatomic parameters were automatically computed by the software per ROI based on the 3D T2-weighted sequence: spinal cord cross-sectional area (CSA) (mm^2), CSF-space (mm^2), spinal canal CSA (mm^2), and – as newly introduced – an adapted maximum canal compromise (aMCC) as measure of the individual's spinal stenosis unrelated to body size. Instead of the application of diameters (mm), according to the commonly used MCC (Nouri et al., 2016), the aMCC used the spinal canal CSA (mm^2) per segment: [(spinal canal CSA one segment above + spinal canal CSA one segment below) ÷ (2 × spinal

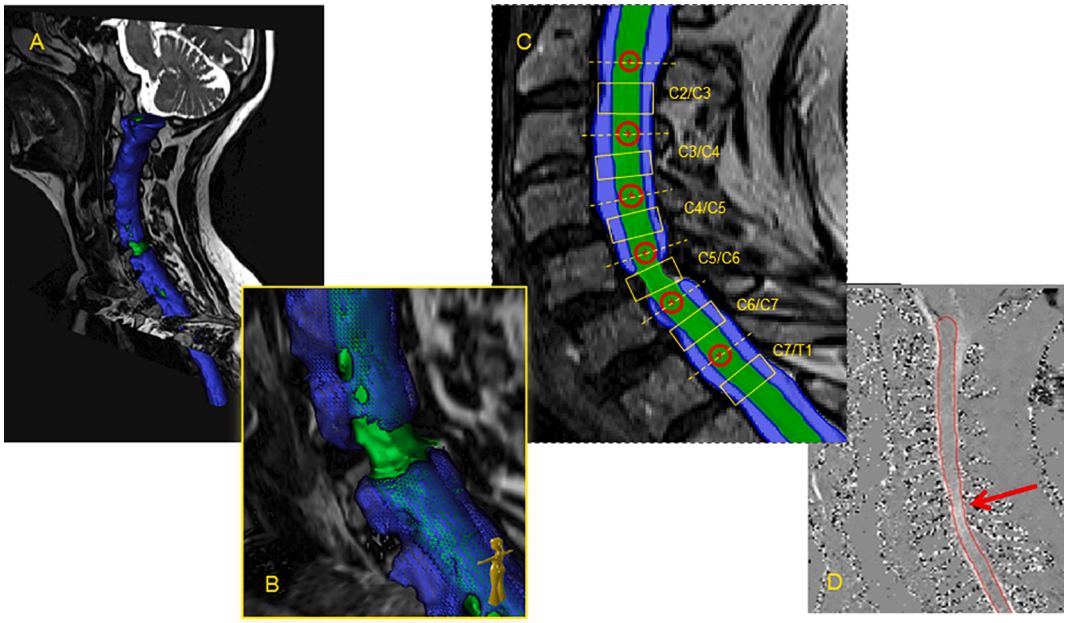

Fig. 1. Examples of MRI data processing. A – 3D T2 SPACE, automated segmentation of subarachnoid space (blue) and spinal cord (green). B – 3D T2 SPACE, image enlargement of the level of stenosis within A. C – magnitude image PC-MRI, segmentation of subarachnoid space (blue) and spinal cord (green) including example of segmental region of interest (yellow squares) covering the middle 1/3 of the spinal cord tissue between two cervical vertebral bodies (red dots). Generation of segmental regions of interests was identical within 3D T2 SPACE images. D – phase difference image PC-MRI, segmented spinal cord (red lines), increased spinal cord movement indicated by light grey at level of stenosis (red arrow). (For interpretation of the references to colour in this figure legend, the reader is referred to the web version of this article.)

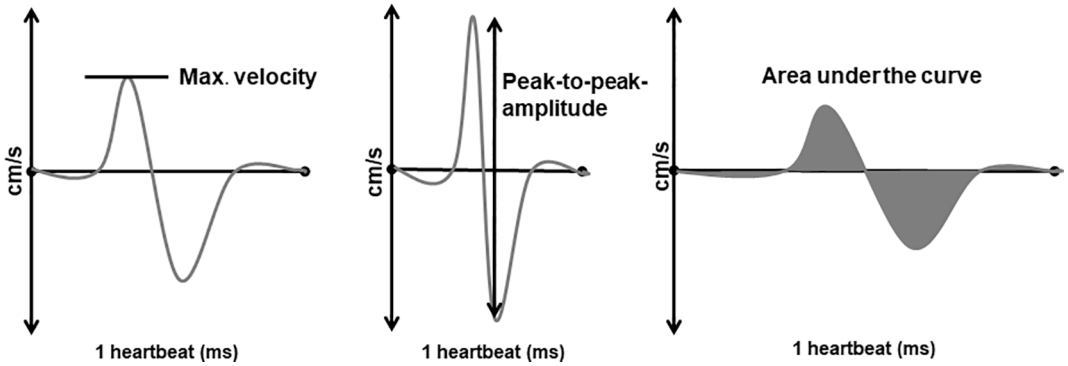

Fig. 2. Schematic diagrams of spinal cord motion and its dynamic parameters. The PC-MRI sequence measures the velocity within approximately 40 time-points per heartbeat, given in cm/s. The maximum velocity (max. velocity) is the highest velocity measured within one heartbeat (left). The peak-to-peak (PTP)-amplitude is the subtraction of highest and lowest peak of the curve, giving more information of the overall extend of the spinal cord motion (middle). The area under the curve (AUC) comprises information of all measured time-points over the duration of one heartbeat (right). By addition of inversed negative values, the total displacement (mm) of the tissue during one heartbeat can be calculated. The duration of the heartbeat is assumed to inversely influence spinal cord dynamics according to literature (schematically demonstrated left to right: shorter duration of the heartbeat causes higher amplitudes and vice versa).

canal CSA at level)].

The angle of the cervical lordosis within the supine positioning of the subjects within the MRI scanner was manually assessed as angle between the reference line over the atlas and the bottom line of the 7th cervical vertebra (Stagnara et al., 1982) using AGFA IMPAX Viewing software®.

2.6. Data validity

Two independent raters (KW, MH) repeated the anatomical labeling process in 15 patients within the same scan for the analysis of inter-rater reliability and of the consistency of the following data-processing within NORA. For analysis of the test–retest-reliability, the sagittal PC-MRI sequence was repeated among 18 patients and each analyzed accordingly within the software. Two independent raters (KW, SFB) measured the angles of cervical lordosis within 15 participants ppaarticip for analysis of inter-rater reliability.

2.7. Statistics

Statistic analysis was conducted by IBM SPSS Statistics®, Version 26. Reliability of repeated measurements was determined via Intra-class Correlation Coefficient (ICC; single measures, two-way mixed effects model, absolute agreement) and classified as "poor" for <0.5, "moderate" for 0.50–0.74, "good" for 0.75–0.9, and "excellent" for >0.9 (Koo and Li, 2016). ICC < 0.5 was not considered acceptable. Data was given as mean and standard deviation (SD). Data was tested upon their distribution (Shapiro-Wilk) and the comparison of groups was done accordingly via *t*-test for normally distributed (nd) data and via Mann-Whitney-*U* test for non-normally distributed (nnd) data. Comparison of variables within groups was calculated via Bonferroni-adjusted post-hoc

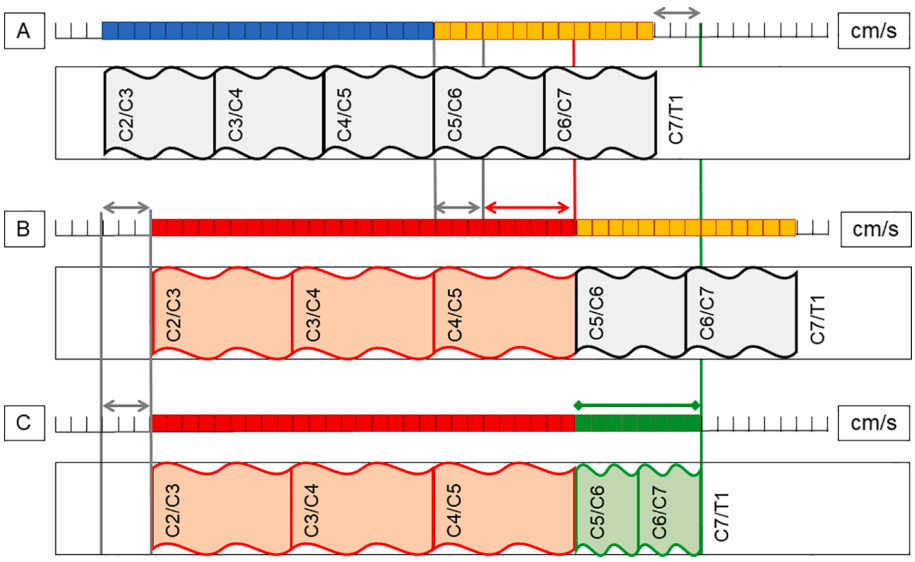

Fig. 3. A – schematic illustration of the cervical spinal segments at the beginning of the heartbeat, amplitude of spinal cord motion measured in cm/s. B – the higher amplitude of spinal cord motion at the segment C5/C6 (red arrow) compared to the segment C2/C3 (grey arrow) results in a stretch of the interjacent spinal cord tissue (red squares). The caudal segments move at the same speed as the segment C5/C6 (yellow squares). Therefore, the caudal spinal cord tissue remains unaffected. C – Segment C5/6 moves at the same speed as demonstrated within B. The spinal cord motion at the segment C7/T1 is as fast as the spinal cord motion at the segment C2/C3 (grey arrow), but less than compared to the segment C5/C6. The interjacent spinal cord tissue becomes compressed (green squares). (For interpretation of the references to colour in this figure legend, the reader is referred to the web version of this article.)

analysis of repeated measures ANOVA upon validation of sphericity. In case of violation of sphericity, Friedmann analysis was conducted and indexed as such. Bivariate correlation was rated by Pearson coefficients. P was required <0.05 to assume significance.

3. Results

3.1. Data validity

The ICC of repeated data processing by the software based on independent manual labelling of segments was moderate for CSF-space at C2/C3 (ICC = 0.724), good for spinal cord CSA at C6/C7 (ICC = 0.799), CSF-space at C7/T1 (ICC = 0.879), and aMCC at C2/C3 (ICC = 0.849). After outlier analysis and exclusion of one case, the before mentioned ICCs were >0.9. The ICCs of all other 32 parameters, including all dynamic parameters, were excellent (ICC > 0.9). Also, the test–retest-reliability of the sagittal PC-MRI scans including consecutive data processing showed mostly excellent and only five good ICCs per dynamic value and segment (ICC range 0.76–0.99, mean 0.90 ± 0.08), with exception of the total displacement at C2/C3 (initial ICC = 0.39, ICC = 0.50 after exclusion of one outlier). In accordance, total displacement at C2/C3 was not used within the further analysis. The agreement of the manual cervical lordosis measurement was excellent (ICC = 0.916).

3.2. Study population

There were no differences in gender (12 male per group) and age (nd, patients: 52.97 ± 12.5 years, controls: 53.21 ± 12.3 years, p = 0.941). Duration of the heartbeat did no differ among groups (nnd, patients: 884 ± 211 ms, controls 953 ± 137 ms, p = 0.347). Mean mJOA score of all patients was 16.7 ± 1.4.

Patients showed significantly reduced spinal canal CSA at each cervical segment compared to controls with an expected minimum at C5/C6 (p < 0.001, each; Figure Supplementary figure 1, spinal canal CSA C5/C6: nd, patients: 71 ± 25 mm^2, controls: 189 ± 42 mm^2, p < 0.001). The aMCC was correspondingly significantly higher among patients at

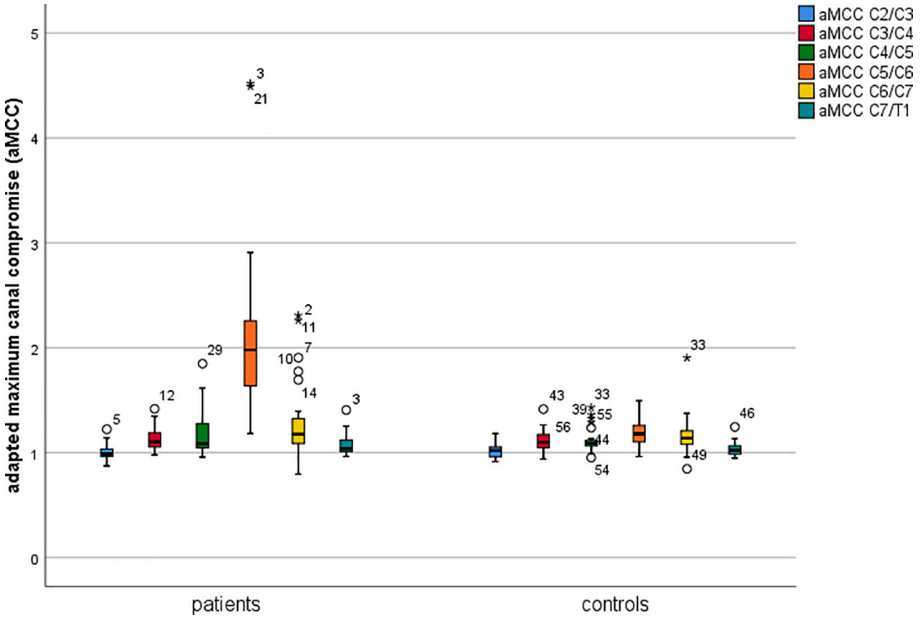

Fig. 4. Boxplot of adapted maximum canal compromise (aMCC) at segments C2/C3 to C7/T1 among patients (left) and controls (right). aMCC at C5/C6 was significantly higher among patients (2.12 ± 0.772, controls: 1.19 ± 0.13, p < 0.001), there was no difference between other levels.

C5/C6 (nnd, patients: 2.1 ± 0.8, controls: 1.2 ± 0.1, p < 0.001), but not different at any other segment (p = 0.228–0.738), emphasizing the fact of monosegmental relevant stenosis at this level (Fig. 4).

3.3. PC-MRI parameters

All dynamic parameters were significantly increased at segments C4/C5, C5/C6, and C6/C7 among patients (Table 1). Both groups displayed a relative increase of dynamic parameters towards C4/C5 and C5/C6, followed by a relative decrease towards C7/T1. This finding remained, when the duration of the heartbeat was considered (total displacement, PTP-amplitude^{HB}).

The pAI was significantly increased among patients at segments C4/C5, C5/C6, and C6/C7 as well, indicating a relevant increase of the local spinal cord motion per segment compared to the individual's spinal cord motion at segment C2/C3 (Fig. 5). The increase of the pAI from C3/C4 to C4/C5 and from C3/C4 to C5/C5 was significant among patients (p = 0.002, p < 0.001, respectively). But also, the decreases of the pAI from C5/C6 to C6/C7 and C7/T1, and from C6/C7 to C7/T1 were significant (p < 0.001, each). This implies an up-building stretch of the spinal cord tissue cranial of the stenosis, followed by a compression caudal of the stenosis (Fig. 3). Among controls, one outlier (case 33) of the pAI variance was observed, that could not be identified by outlier analysis of any other dynamic or anatomic data, but by aMCC at C6/C7 (Fig. 4).

3.4. Relevance across the cervical spinal cord

In accordance with previous reports (Hupp et al., 2019; Winklhofer et al., 2014), spinal cord motion relevantly differed between cervical segments among controls (Supplement 2). At an overall lower level of spinal cord motion than compared to patients, a cranio-caudal increase was observed towards the cervical segments C4/C5 and C5/C6 (p < 0.001–0.011), followed by a decrease towards C7/T1 (p < 0.001–0.026). Motion at the most cranial and caudal segments were similar.

Among patients, spinal cord motion differed more often in-between cervical segments and its pathophysiological alterations caused more far range effects across the cervical spinal cord compared to controls (Fig. 6, Supplement 2): e.g. the number of significant differences between segments for the PTP-amplitude^{HB} was 10/15 within patients vs. 4/15 within controls (p = 0.044). Also, whereas controls showed similar spinal cord motion at C2/C3 and C6/C7 (e.g. PTP-amplitude^{HB} C2/C3 6.1 ± 2.1 mm vs. PTP-amplitude^{HB} C6/C7 5.5 ± 3.1 mm, p = 1.00), there was a significant far range effect among patients (e.g. PTP-amplitude^{HB} C2/C3 6.4 ± 2.5 mm vs. PTP-amplitude^{HB} C6/C7 9.7 ± 5.3 mm, p = 0.018).

Table 1
Comparison of dynamic parameters per segment, values given in mean and standard deviation (SD). HB – heartbeat, PTP – peak-to peak, PTP-amplitude^{HB} – PTP-amplitude × duration of the heartbeat. Significant changes (p < 0.05) are marked in bold type.

	Segment	Patients		Controls		
		mean	SD	mean	SD	p
Maximum velocity (cm/s)	C2/C3	0.49	0.20	0.45	0.17	0.405
	C3/C4	0.59	0.24	0.51	0.21	0.234
	C4/C5	**0.69**	**0.31**	**0.51**	**0.23**	**0.018**
	C5/C6	**0.96**	**0.52**	**0.49**	**0.22**	**<0.001**
	C6/C7	**0.66**	**0.30**	**0.39**	**0.20**	**<0.001**
	C7/T1	0.48	0.28	0.37	0.20	0.107
PTP-amplitude (mm/s)	C2/C3	7.26	2.38	6.44	2.21	0.240
	C3/C4	8.73	2.61	7.73	2.84	0.146
	C4/C5	**11.01**	**4.09**	**7.93**	**3.41**	**0.002**
	C5/C6	**14.56**	**7.25**	**8.08**	**3.40**	**<0.001**
	C6/C7	**10.78**	**5.07**	**6.97**	**3.34**	**<0.001**
	C7/T1	8.28	4.59	6.66	3.42	0.065
Total displacement (mm)	C3/C4	1.18	0.34	1.09	0.27	0.292
	C4/C5	**1.52**	**0.52**	**0.99**	**0.25**	**<0.001**
	C5/C6	**1.96**	**1.43**	**1.01**	**0.27**	**<0.001**
	C6/C7	**1.44**	**0.64**	**0.99**	**0.40**	**<0.001**
	C7/T1	**1.22**	**0.42**	**1.05**	**0.60**	**0.025**
PTP-amplitude^{HB} (mm)	C2/C3	6.43	2.53	6.09	2.08	0.570
	C3/C4	7.80	3.12	7.25	2.56	0.441
	C4/C5	**10.01**	**4.58**	**7.43**	**3.07**	**0.006**
	C5/C6	**13.15**	**7.18**	**7.59**	**3.07**	**0.001**
	C6/C7	**9.72**	**5.251**	**5.54**	**3.08**	**0.005**
	C7/T1	7.36	4.434	6.37	3.56	0.174
PTP-amplitude index (pAI)	C3/C4	1.23	0.22	1.21	0.21	0.957
	C4/C5	**1.64**	**0.66**	**1.24**	**0.38**	**0.003**
	C5/C6	**2.15**	**1.04**	**1.29**	**0.50**	**<0.001**
	C6/C7	**1.60**	**0.77**	**1.09**	**0.36**	**0.001**
	C7/T1	1.21	0.67	1.07	0.54	0.301

3.5. Correlations to anatomic data

Among controls, age negatively correlated to the spinal cord CSA at segments C2/C3 to C6/C7 (r = −0.680 to −0.440, p < 0.001–0.017). Among patients, the negative correlation remained only at segments C2/C3 (r = −0.461, p = 0.012) and C3/C4 (r = −0.380, p = 0.048) and dissolved expectedly at segments C5/C6 and C6/C7. Controls showed a positive relation of the angle of the cervical lordosis to dynamic data at C4/C5, C5/C6 and C6/C7 (max. velocity: C4/C5–r = 0.408, p = 0.030, C5/C6–r = 0.444, p = 0.016, C6/C7–r = 0.428, p = 0.020; PTP-amplitude: C4/C5–r = 0.415, p = 0.025, C5/C6–r = 0.478, p = 0.009, C6/C7–r = 0.510, p = 0.005, PTP-amplitude^{HB}: C4/C5–r = 0.404, p = 0.030, C5/C6–r = 0.463, p = 0.011, C6/C7–r = 0.493, p = 0.007). There were no correlations between the angle of lordosis and dynamic parameters among patients. Dynamic spinal cord parameters showed a tendency towards a negative relationship to anatomic parameters among controls; significant relations were found between pAI at C4/C5, C5/C6 and C6/C7 and the spinal canal CSA at C4/C5 and C5/C6 (pAI C4/C5 to spinal canal CSA C4/C5: r = −0.038, p = 0.045, C5/C6: r = −0.410, p = 0.027, C6/C7: r = -0.547, p = 0.002, pAI C5/C6 to spinal canal CSA C6/C7: r = −0.483, p = 0.008, pAI C6/C7 to spinal canal CSA C5/C6: r = −0.480, p = 0.008, C6/C7: r = −0.518, p = 0.004, pAI C7/T1 to spinal canal CSA C6/C7: r = −0.374, p = 0.046). Among patients, pAI at C7/T1 correlated negatively to spinal canal CSA at C7/T1 (r = −0.374, p = 0.046).

The aMCC at C5/C6 correlated positively to the total displacement at C3/C4 (r = 0.483, p = 0.009) and C4/C5 (r = 0.393, p = 0.038), as well as to the pAI C3/C4 (r = 0.427, p = 0.029) among patients. There was no correlation to dynamic parameters at segment C5/C6. Also, additional analyses upon Spearman correlation coefficients, which are less dependent on linear relations, did not reveal a trend.

4. Discussion

This is the first study to describe a significantly increased mechanical stress on the cervical spinal cord tissue remote from focal cervical spinal stenosis. The spinal cord tissue is object of an up-building mechanical stretch cranial of the stenosis and of compressive effects caudal of the stenosis. The focus of these effects remains at the segments adjacent to the stenosis. Still, far range alterations of spinal cord motion up to four segments apart can be observed among patients.

Furthermore, data of healthy controls suggest a physiological evolution of spinal cord motion across the cervical spine, relations to spinal canal CSA and angle of cervical lordosis in supine positioning. Within patients, these observed relations dissolve, implicating relevant pathodynamic alterations within the spinal canal.

Spinal cord motion within the cervical spinal canal has been described in physiological (systolic cranial and diastolic caudal motion) and pathophysiological conditions within cervical spinal stenosis (e.g. Wolf et al., 2018; Hupp et al., 2019; Figley and Stroman, 2007; Tanaka et al., 1998). The exact origin of the physiological spinal cord dynamic is still unclear. Besides known antidromic relation to CSF-flow (e.g.

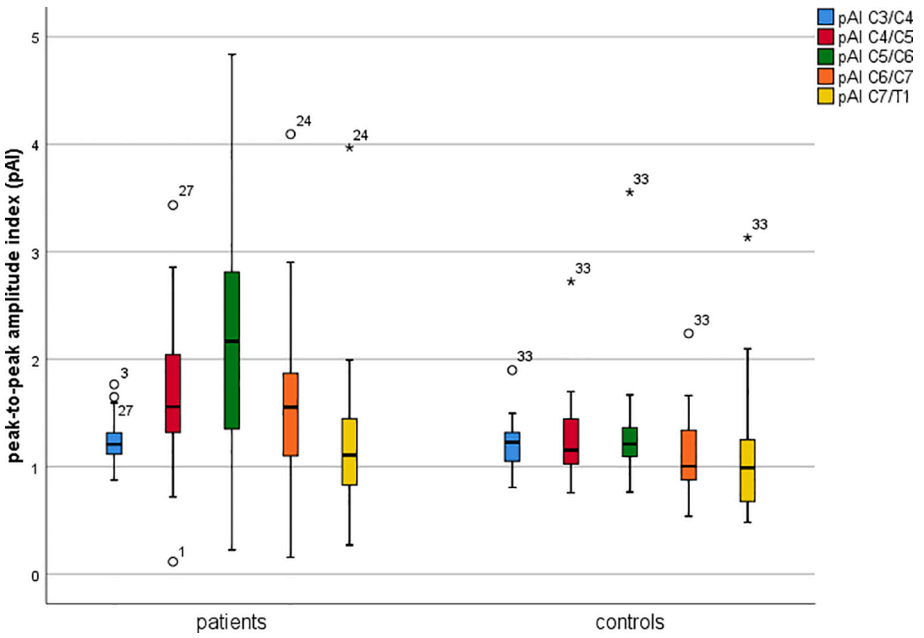

Fig. 5. Boxplot of the peak-to-peak (PTP)-amplitude index (pAI) at segments C3/C4 to C7/T1 among patients (left) and controls (right). The pAI relates the PTP-amplitude per segment C3/C4–C7/T1 to the individual's PTP-amplitude at C2/C3 and therefore gives information upon the relative increase or decrease of spinal cord motion per segment despite possible interindividual differences of body size or spinal canal configuration. Additionally, it reveals information upon stretching or compressive effects on the spinal cord tissue. The pAI at segments C4/C5, C5/C6 and C6/C7 was significantly higher among patients ($p = 0.003$, $p < 0.001$, $p = 0.001$, respectively). Among patients, the increase of the pAI from C3/C4 to C4/C5 and C4/C5 to C5/C6 was significant ($p = 0.002$, $p < 0.001$, respectively) (Fig. 3, B); the decrease of pAI from C5/C6 to C6/C7, and from C6/C7 to C7/T1 was significant as well ($p < 0.001$ each) (Fig. 3, C). This implied a relevant stretch of spinal cord tissue cranial to the stenosis and compression of the tissue caudal of the stenosis.

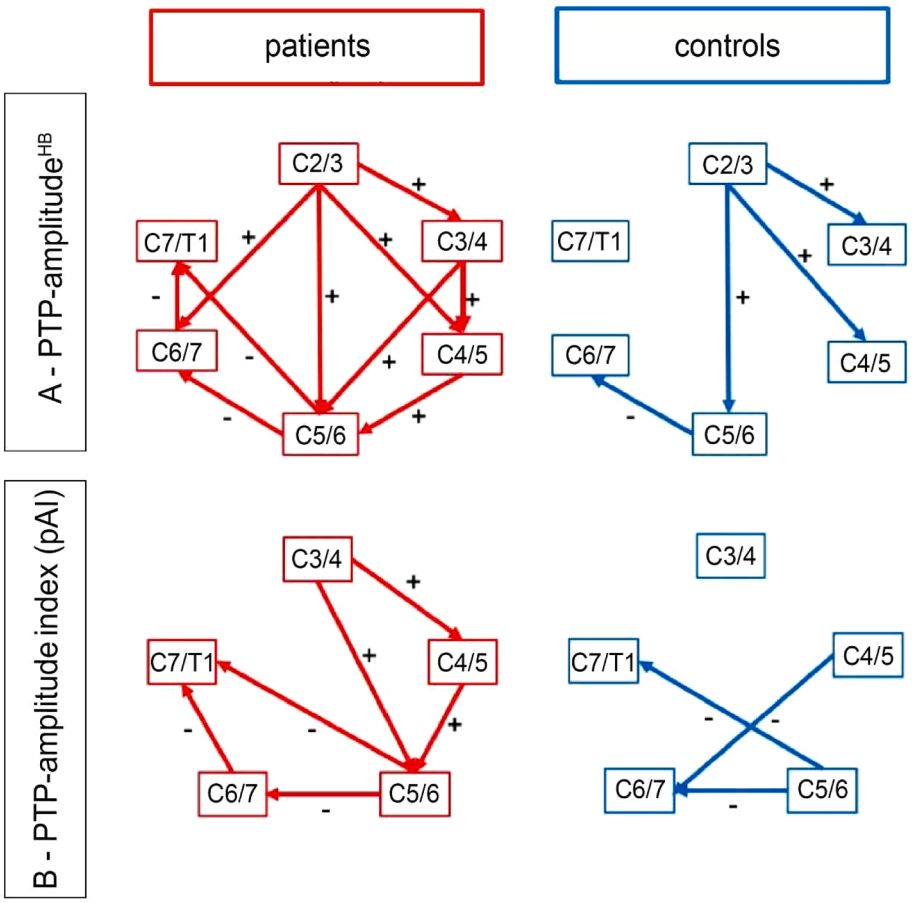

Fig. 6. Significant differences of mean ± SD of the (A) peak tot peak (PTP)-amplitude^{HB} and the (B) PTP-amplitude index (pAI) between all single segments across the cervical spinal cord. Red – patients, blue – controls; "+" indicating a significant increase of spinal cord motion from cranial to caudal segment, "–" indicating a significant decrease of spinal cord motion from cranial to caudal segment. (For interpretation of the references to colour in this figure legend, the reader is referred to the web version of this article.)

Vavasour et al., 2014), influence of deep breathing and the heart rate (e.g. Figley and Stroman, 2007; Winklhofer et al., 2014), an impact of local expansion of the arteries into the subarachnoid space is assumed (Matsuzaki et al., 1996). Taking different aspects of influencing factors into account, that have been discussed before (e.g. Wolf et al., 2018, 2019; Hupp et al., 2019), we hypothesized, that – as the subarachnoid space diminishes and the CSF-flow is accelerated (Bunck et al., 2011) – the antidromic pressure gradients caused the increased spinal cord motion. The analyses of anatomic correlations to dynamic data surprises, as there was no significant correlation between spinal cord motion at C5/

C6 to the severity of the stenosis measured as aMCC at C5/C6. On the one hand, this might indicate influencing factors beyond local anatomy, such as e.g. the compliance capacity of the spinal canal itself. On the other hand, the data might implicate, that the disorganization of the physiological cord motion patterns might occur early within the course of the disease, even at stages of moderate stenosis. This emphasizes, that measurements of spinal cord motion contain information beyond anatomical imaging.

The presented methods and analysis tools are a novelty within the field of clinical research applying spinal PC-MRI and are at a very high level of reliability. For a first time, we introduced an automated segmentation of the subarachnoid space and the spinal cord with application of automated ROIs and subsequent analysis tools within NORA.

Several clinical studies on cervical spinal stenosis have addressed the topic of altered spinal cord motion applying PC-MRI (Wolf et al., 2018; Vavasour et al., 2014; Chank et al., 2014). As demonstrated before, the test–retest-reliability of PC-MRI measurements analyzed by manual segmentation are at a high level (Hupp et al., 2019). In contrast to formerly presented data by Hupp et al. (2019) with good test–retest-reliability at all segments but C7/T1, the currently presented results could show good reliability for all dynamic parameters throughout all cervical segments but total displacement at C2/3. We suspect that the low test–retest-variability of the total displacement at C2/3 might be due to lower spinal cord velocities at this segment and therefore less sensitivity of the current PC-MRI sequence setting with a VENC of 5 cm/s. Within diseases expecting lower spinal cord dynamics (e.g. with focus on more cranial pathophysiological alterations, e.g. Chiari malformation), a VENC of 3–4 cm/s might be advisable. All other data showed high inter-rater and test–retest-reliability at all levels including the current method of data processing (segmentation, phase-drift-correction, manual labeling, generation of ROIs and computation of values). This results within a methodology, which is altogether less susceptible for errors and robust despite degenerative canal deformation. Compared to former analyses of reliability of other automated spinal cord segmentation tools, the ICC of spinal cord CSA at C6/C7 is currently lower than previously reported (e.g. (Papinutto and Henry, 2019; De Leener et al., 2015). As the ICC improved tremendously after exclusion of one outlier, we suspect the low inter-rater agreement to be caused by the manual labeling process. Improvement should be accomplished by automated segmental labeling.

Within this upcoming field, a large variety of scan protocols (without phase-drift correction, axial vs. sagittal scans, use of different dynamic parameter) complicated a comparison of values. We propose to use the current standard of phase-drift corrections as elaborated above and applied within our data processing (Gatehouse et al., 2012). Whether axial and sagittal scans can be compared without correction of the angle of cervical lordosis, needs to be investigated. The dynamic parameters need to be interpreted regarding the value they express: absolute values as the maximum velocity and PTP-amplitude are easily to assess, but – as the duration of the diastolic phase increases with the duration of the heartbeat – an inverse relationship must be assumed according to literature (Enzmann and Pelc, 1992; Bradley et al., 2016) (Fig. 2). Therefore, parameters including information of the heartbeat should be rather suitable for interindividual comparison, like total displacement and the newly introduced parameter PTP-amplitude^{HB}.

The index of motion data per cervical segment in relation to the unaffected segment C2/3 gives additional relative information on segmental alterations across the cervical spine unrelated to intra-individual unknown differences (e.g. body size) (Wolf et al., 2018). Within the sagittal imaging setting, the pAI can be used due to the fact of unchanged duration of the average heartbeat within one MRI sequence. But in case of subsequent imaging, the heartbeat should be considered per scan and therefore parameters like PTP-amplitude^{HB} or total displacement should be used when computing an index.

Within the healthy condition, a physiological increase of spinal cord motion towards the segment C5/C6 as well as segmental differences of spinal cord motion have been noted before (Hupp et al., 2019; Winklhofer et al., 2014). Our data supported this finding and the conclusion, that further comparison between patients and controls can only be performed per cervical segment.

The relation of increased spinal cord motion to a higher angle of the cervical lordosis within the supine positioning in the scanner among controls can be explained by the direction of the velocity measurements. If the direction of the actual moving substance is parallel to the encoding direction, the true data can be captured, whereas velocities are seemingly lower in case of non-parallel vectors. This would imply that the spinal cord motion at the segments of maximum cervical lordosis (C4/C5, C5/C6) might be even higher than currently measured, as a higher angle indicates non-parallel motion. Despite missing linear correlation among patients possibly due to the high dynamic effects of the stenosis itself, we expect that this would be true for both, patients and controls. As there was no difference of the angle of cervical lordosis between groups, this should not affect the current dataset, but might be a topic that needs to be addressed within future protocols.

4.1. Limitations

This study employs sound methods and clear defined cohorts. Thus, this study gives further insights on the evolution of intraspinal dynamics and the pathodynamic mechanical stresses on the spinal cord tissue that likely seem to play a role in spinal cord deterioration. Effects on non-symptomatic spinal stenosis were not topic of this study but need to be addressed within further trials in order to evaluate the dynamic spinal cord motion parameters towards their value within clinical diagnostics. This is underlined by the incidental outlier (case 33) and the relatively increased aMCC at C6/C7. The study does not answer questions on relations to clinical impairment. Due to the number of participants, data on physiological conditions need to be interpreted carefully. Still, this study gives new insights on methods, handling of parameters and pathodynamic alterations within the assessment and interpretation of spinal cord motion in cervical spinal stenosis using PC-MRI.

5. Conclusion

The presented data revealed pathodynamic stress on spinal cord tissue across the entire cervical spinal cord due to focal stenosis. The increase of spinal cord motion specifically at level of stenosis has been described before Wolf et al. (2018) and could be reproduced. In addition, the significant differences of the adjacent segments C4/C5 and C6/C7 between the two groups demonstrated relevantly elevated spinal cord motion at these segments as well. Furthermore, the presented data implied far range effects across the cervical spinal cord. The dynamic data indicated an up-building stretch upon the spinal cord tissue beginning at segment C3/C4 and significantly increasing towards the stenotic segment C5/C6. The decrease of the dynamic parameters from C5/C6 to C7/T1 indicated a relevant caudal compression of the tissue. As the physiological association to anatomic data and age diminished among patients, the impact of the alteration across the cervical spinal canal becomes emphasized.

Due to the extent of observed pathodynamic alterations, we expect these findings to be clinically relevant.

Funding

Our study received funding from the German Spine Foundation (number 12/2017) and the program “Clinical Studies 2019” of the Faculty of Medicine, University of Freiburg, Germany (number: 3091331904).

The article processing charge was funded by the Baden-Württemberg Ministry of Science, Research and Art and the University of Freiburg in the funding programme Open Access Publishing.

CRediT authorship contribution statement

Katharina Wolf: Conceptualization, Data curation, Formal analysis, Funding acquisition, Investigation, Methodology, Project administration, Validation, Visualization, Writing - original draft. **Marco Reisert:** Formal analysis, Methodology, Validation, Software, Conceptualization, Supervision, Writing - review & editing. **Saúl Felipe Beltran:** Formal analysis, Validation, Writing - review & editing. **Jan-Helge Klingler:** Conceptualization, Methodology, Validation, Writing - review & editing. **Ulrich Hubbe:** Conceptualization, Funding acquisition, Methodology, Writing - review & editing. **Axel J. Krafft:** Conceptualization, Funding acquisition, Methodology, Project administration, Resources, Software, Validation, Writing - review & editing. **Karl Egger:** Conceptualization, Methodology, Validation, Writing - review & editing. **Marc Hohenhaus:** Conceptualization, Data curation, Funding acquisition, Investigation, Methodology, Project administration, Validation, Writing - review & editing.

Declaration of Competing Interest

A. J. Krafft is currently employed at Siemens Healthcare GmbH, Erlangen, Germany; he contributed to the study while being employed at the Department of Neuroradiology, Medical Center – University of Freiburg, Faculty of Medicine, University of Freiburg, Germany.

The authors declare that they have no known competing financial interests or personal relationships that could have appeared to influence the work reported in this paper.

Acknowledgments

We thank D. Gruninger, Department of Neurosurgery, and H. Mast, Department of Neuroradiology for their patience and support. Also, we thank G. Wolf for his assistance on MK.

Appendix A. Supplementary data

Supplementary data to this article can be found online at https://doi.org/10.1016/j.nicl.2021.102580.

References

Bunck, A.C., et al., 2011. Magnetic resonance 4D flow characteristics of cerebrospinal fluid at the craniocervical junction and the cervical spinal canal. Eur. Radiol. 21 (8), 1788–1796.

Wolf, K., et al., 2018. In cervical spondylotic myelopathy spinal cord motion is focally increased at the level of stenosis: a controlled cross-sectional study. Spinal Cord 56 (8), 769–776. https://doi.org/10.1038/s41393-018-0075-1.

Markl, M., et al., 2012. 4D flow MRI. J. Magn. Reson. Imaging 36 (5), 1015–1036.

Dyverfeldt, P., et al., 2015. 4D flow cardiovascular magnetic resonance consensus statement. J. Cardiovasc. Magn. Reson. 17 (1) https://doi.org/10.1186/s12968-015-0174-5.

Yamada, A., et al., 2015. Current and emerging MR imaging techniques for the diagnosis ad management of CSF flow disorders: a review of phase-contrast and time-spatial labeling inversion pulse. Am. J. Neuroradiol. 36, 623–630.

Vavasour, I.M., et al., 2014. Increased spinal cord movements in cervical spondylotic myelopathy. Spine J. 14 (10), 2344–2354.

Chank, H.S., et al., 2014. Increased flow signal in compressed segments of the spinal cord in patients with cervical spondylotoc myelopathy. Spine 39, 2136–2142.

Hupp, M., et al., 2019. Segmental differences of cervical spinal cord motion: advancing from confounders to a diagnostic tool. Sci. Rep. 9 (1) https://doi.org/10.1038/s41598-019-43908-x.

Wolf, K., et al., 2019. Assessment of spinal cord motion as a new diagnostic MRI-parameter in cervical spinal canal stenosis: study protocol on a prospective longitudinal trial. J Orthop Surg Res. 14 (1) https://doi.org/10.1186/s13018-019-1381-9.

Kato, S., et al., 2015. Comparison of the Japanese Orthopaedic Association (JOA) score and modified JOA (mJOA) score for the assessment of cervical myelopathy: a multicenter observational study. PLoS One 10 (5).

nora-imaging. (Online) <http://www.nora-imaging.org>.

Zhao, B., et al., 2019. A multi-scale strategy for deep semantic segmentation with convolutional neural networks. Neurocomputing 365, 273–284. https://doi.org/10.1016/j.neucom.2019.07.078.

Gatehouse, P.D., et al., 2012. A multi-center inter-manufacturer study of the temporal stability of phase-contrast velocity mapping background offset errors. J. Cardiovasc. Magn. Reson. 14 (1), 72. https://doi.org/10.1186/1532-429X-14-.

Enzmann, D.R., Pelc, N.J., 1992. Brain motion: measurement with phase-contrast MR imaging. Radiology 185 (3), 653–660.

Bradley, W.G., Haughton, V., Mardal, K.A., 2016. Cerebrospinal fluid flow in adults. Hand. Clin. Neurol. 135, 591–601.

Nouri, A., et al., 2016. Magnetic resonance imaging assessment of degenerative cervical myelopathy: a review of structural changes and measurement techniques. Neurosurg. Focus 40 (6), E5. https://doi.org/10.3171/2016.3.FOCUS1667.

Stagnara, P., et al., 1982. Reciprocal angulation of vertebral bodies in a sagittal plane: approach to references for the evaluation of kyphosis and lordosis. Spine (Phila Pa 1976) 7 (4), 335–342. https://doi.org/10.1097/00007632-198207000-00003.

Koo, T.K., Li, M.Y.A., 2016. Guideline of selecting and reporting intraclass correlation coefficients for reliability research [published correction appears in J Chiropr Med. 2017, 2016, 16(4):346]. J Chiropr Med. 15 (2), 155–163. https://doi.org/10.1016/j.jcm.2016.02.012.

Winklhofer, S., et al., 2014. Spinal cord motion: influence of respiration and cardiac cycle. Fortschr. Röntgenstr. 136, 1116-1021.

Figley, C.R., Stroman, P.W., 2007. Investigation of human cervical and upper thoracic spinal cord motion: implications for imaging spinal cord structure and function. Magn. Reson. Med. 58 (1), 185–189.

Tanaka, H., et al., 1998. Transition of the craniocaudal velocity of the spinal cord: from cervical segment to lumbar enlargement. Invest. Radiol. 33 (3), 141–145.

Matsuzaki, H., et al., 1996. The origin and significance of spinal cord pulsation. Spinal Cord. 34 (7), 422–426.

Papinutto, N., Henry, R.G., 2019. Evaluation of Intra- and Interscanner Reliability of MRI Protocols for Spinal Cord Gray Matter and Total Cross-Sectional Area Measurements. J. Magn. Reson. Imaging 49 (4), 1078–1090. https://doi.org/10.1002/jmri.26269.

De Leener, B., Cohen-Adad, J., Kadoury, S., 2015. Automatic segmentation of the spinal cord and spinal canal coupled with vertebral labeling. IEEE Trans. Med. Imaging. 34 (8), 1705–1718. https://doi.org/10.1109/TMI.2015.2437192.